WIND-TUNNEL MEASUREMENTS OF THE AERODYNAMIC DAMPING AND OSCILLATORY STABILITY IN PITCH OF A SPHERE AT MACH NUMBERS FROM 0.20 TO 4.63

A Thesis

Presented to

The Faculty of the Department of Physics

The College of William and Mary in Virginia

In Partial Fulfillment

Of the Requirements for the Degree of

Master of Arts

By

Robert Ashworth Kilgore

August 1963

WIND-TUNNEL MEASUREMENTS OF THE AERODYNAMIC DAMPING AND OSCILLATORY STABILITY IN PITCH OF A SPHERE AT MACH NUMBERS FROM 0.20 TO 4.63

A Thesis

Presented to

The Faculty of the Department of Physics

The College of William and Mary in Virginia

In Partial Fulfillment

Of the Requirements for the Degree of

Master of Arts

By

Robert Ashworth Kilgore

August 1963

APPROVAL SHEET

This thesis is submitted in partial fulfillment of

the requirements for the degree of

Master of Arts

Author

Approved, August 1963:

J. D. Lawrence, Ph.D.

Melvin A. Pittman, Ph.D.

George W. Crawford, Ph.D.

TABLE OF CONTENTS

Chapter | Page

LIST OF FIGURES

ABSTRACT

The aerodynamic damping and oscillatory stability in pitch of a sphere at selected Mach numbers from 0.20 to 4.63 have been determined experimentally by using a small-amplitude forced-oscillation test technique. The data obtained for oscillation centers forward of, coincident with, and rearward of the geometric center of the sphere are presented as a function of mean angle of attack. In addition to the test results, some details of the test technique are included for the benefit of other workers in the same field who may be interested. Nomenclature suited to this type of wind-tunnel test is used in the development of the equations which were used to reduce the measured aerodynamic characteristics to nondimensional form.

Appendix II presents a method by which the small-amplitude forced-oscillation test technique may be used to separate the two derivatives which are combined in the oscillatory-stability parameter.

WIND-TUNNEL MEASUREMENTS OF THE AERODYNAMIC DAMPING AND OSCILLATORY STABILITY IN PITCH OF A SPHERE AT MACH NUMBERS FROM 0.20 TO 4.63

INTRODUCTION

A sphere having linear motion with respect to a fluid has been the subject of many theoretical and experimental works in aerodynamics and hydrodynamics. The sphere, being the most basic of three-dimensional shapes, is often used as a calibration device in wind tunnels because so much information exists concerning the flow over the sphere and the forces on the sphere as a function of wind-tunnel variables.

A lack of experimental information concerning the aerodynamic damping and oscillatory stability of spheres prompted this program to measure the damping and oscillatory stability characteristics in pitch of a sphere by using a small-amplitude forced-oscillation test technique.

In addition to the test results, some details of the test technique are included in this paper for the benefit of other workers in the same field who may be interested. The nomenclature employed herein differs from the nomenclature employed by flight aerodynamicists. The desirability of this departure from convention is explained in chapter I where the equations which were used to reduce the measured aerodynamic characteristics to nondimensional form are developed.

Appendix II presents a method by which the small-amplitude forced-oscillation test technique may be used to separate the two derivatives which are combined in the oscillatory-stability parameter.

CHAPTER I

EQUATIONS FOR REDUCTION OF DATA

1.1 Preliminary Remarks

The complete description of the motion of a rigid body generally requires a set of six simultaneous differential equations. A single differential equation suffices for the mathematical description of the motion of a rigid body if one point in the body is fixed in the laboratory and freedom is restricted to rotation about a single axis. Because the technique which was used for these tests limits the motion of the rigid body to small-amplitude angular oscillations about the body Y-axis (pitch axis) the problem is reduced to setting up and solving the differential equation of the oscillating system and then solving the resulting algebraic equation for the aerodynamic characteristics of the rigid body. This should be done in such a way that the aerodynamic characteristics of the rigid body are expressed in terms of conventional nondimensional aerodynamic derivatives equated to measurable quantities.

Unfortunately, the conventional nondimensional aerodynamic derivatives are intimately associated with airplane configurations. This association has led to the rather restrictive assumption that the angle of attack is very near 0°. (See, for example, refs. 1 and 2.)

When this and certain other less restrictive assumptions are made, the dimensional aerodynamic damping coefficient C_{aero}, as measured on a rigid body in a wind tunnel by the small-amplitude forced-oscillation technique can be expressed in a nondimensional form as the "damping-in-pitch parameter" $C_{m_q} + C_{m_{\dot{\alpha}}}$. Two nondimensional aerodynamic derivatives are used to represent the single dimensional damping-in-pitch coefficient because due account is taken of the fact that, as explained in reference 2, damping in pitch for a free-flying airplane can arise from both q and $\dot{\alpha}$ even though when using the forced-oscillation technique in a conventional wind tunnel $q = \dot{\alpha}$. Similarly, the usual nondimensional form of $(K - I\omega^2)_{aero}$ is the "oscillatory-longitudinal-stability parameter" $C_{m_\alpha} - \left(\frac{\omega d}{V}\right)^2 C_{m_{\dot{q}}}$. A serious problem arises in deriving these expressions when no assumption is made concerning the magnitude of angle of attack. There is then no rigorous and logical way of expressing the dimensional aerodynamic characteristics in terms of the conventional nondimensional aerodynamic partial derivatives.

Rather than trying to express the measured dimensional aerodynamic characteristics of a rigid body in terms of possible free-flight variables, they will herein be expressed in terms of the variables actually measured in the wind tunnel in a manner similar to that of reference 3, with no restrictions being placed on angle of attack. Thus, the damping-in-pitch parameter is expressed as $C_{m_{\dot{\theta}}}$ and the oscillatory-longitudinal-stability parameter is expressed as $C_{m_\theta} - \left(\frac{\omega d}{V}\right)^2 C_{m_{\ddot{\theta}}}$ where θ is the one angular degree of freedom allowed the model in the wind tunnel. This procedure presents no difficulties because at any mean angle of attack the dimensional values of C_{aero} and $(K - I\omega^2)_{aero}$ are immediately available when their respective nondimensional forms are multiplied by the proper dimensionalizing factors.

1.2 The Differential Equation of Motion

Considerable attention will be given to setting up the differential equation for the rigid body in order to emphasize the fundamental relationships between the nondimensional aerodynamic derivatives and the more familiar mechanical concepts of stiffness, damping, and inertia.

The analysis of this torsional system is based upon Newton's second law in the form

$$\sum M = I\ddot{\theta} \tag{1}$$

where $\sum M$ is the summation of the moments of force applied to the rigid body, I is the mechanical moment-of-inertia coefficient of the rigid body, and $\ddot{\theta}$ is the instantaneous angular acceleration of the rigid body.

As will be explained in section 2.12, the body being tested (the model) is mounted on the oscillation-balance mechanism. The combination of the model, a portion of the oscillation balance forward of the moment sensing strain-gage bridges, and the mechanical spring of the oscillation-balance mechanism forms a "model system" which has lumped mechanical characteristics of torsional stiffness, K, viscous damping, C, and moment of inertia, I.

A sinusoidal forcing function is imposed upon the model system by using a rigid mechanical device (described in section 2.12) to produce oscillations in pitch.

$$\text{Forcing function} = Me^{i\omega t} \tag{2}$$

This forcing function produces a time-dependent change in the angular position of the model system with respect to the supporting sting such that

Instantaneous angular displacement = θ

Instantaneous angular velocity = $\dot{\theta}$

Instantaneous angular acceleration = $\ddot{\theta}$

The coefficient of the mechanical torsional stiffness, K, and the coefficient of the mechanical viscous damping, C, for the model system are both positive and give rise to torques

$$\text{and} \quad \left.\begin{array}{l} \text{Torque due to angular displacement} = -K\theta \\ \text{Torque due to angular velocity} = -C\dot{\theta} \end{array}\right\} \tag{3}$$

The negative sign on $K\theta$ indicates that the torque due to angular displacement of the mechanical spring acts in opposition to the angular displacement and likewise the negative sign on $C\dot{\theta}$ indicates that the torque due to angular velocity acts in opposition to the velocity.

The static pitching moment which would exist if the model were at any angle of attack other then the trim angle of attack (angle of attack where $C_m = 0$) will be a torque about the axis of oscillation. This torque need not be considered in the equation of motion because it is exactly balanced by its equilibrant imposed on the model by the supporting sting. (The model is forced by the sting to be "trimmed" at each mean angle of attack at which data are taken.)

In a manner similar to that used in reference 2, the aerodynamic torques which arise from the motion of the model are expressed as functions of instantaneous angular displacement, instantaneous angular velocity, and instantaneous angular acceleration in the form

$$\sum M_{aero} = \frac{\partial M}{\partial \theta}\theta + \frac{\partial M}{\partial \dot{\theta}}\dot{\theta} + \frac{\partial M}{\partial \ddot{\theta}}\ddot{\theta} \tag{4}$$

Incorporating equations (2), (3), and (4) into equation (1) gives

$$\underbrace{\frac{\partial M}{\partial \theta}\theta + \frac{\partial M}{\partial \dot{\theta}}\dot{\theta} + \frac{\partial M}{\partial \ddot{\theta}}\ddot{\theta}}_{\substack{\text{aerodynamic}\\ \text{torques}}} \underbrace{- K\theta - C\dot{\theta}}_{\substack{\text{mechanical}\\ \text{torques}}} \underbrace{+ Me^{i\omega t}}_{\substack{\text{forcing}\\ \text{function}}} = I\ddot{\theta} \tag{5}$$

Combining coefficients of like terms and rearranging gives the desired differential equation of motion of the model system which is a typical nonhomogeneous linear differential equation of the second order with constant coefficients

$$\left(I - \frac{\partial M}{\partial \ddot{\theta}}\right)\ddot{\theta} + \left(C - \frac{\partial M}{\partial \dot{\theta}}\right)\dot{\theta} + \left(K - \frac{\partial M}{\partial \theta}\right)\theta = Me^{i\omega t} \tag{6}$$

Before equation (6) is solved it is convenient to convert the dimensional pitching moment M to a nondimensional pitching-moment coefficient C_m.

It is shown in reference 4 by dimensional analysis that the force acting on solids moving through fluids can be expressed in the form

$$\text{Force} = F = C_F \frac{1}{2} \rho V^2 A$$

where C_F is a nondimensional force coefficient.

Since a moment (of force) is the product of a force and a length, a moment can be expressed in terms of a nondimensional moment coefficient as

$$\text{Moment} = (\text{force})(\text{length}) = \left(C_M \frac{1}{2} \rho V^2 A\right)(\text{length}) \tag{7}$$

where C_M is a nondimensional moment coefficient.

The length on the right-hand side of equation (7) is usually chosen to be the length, d, which appears in the definition of Reynolds number. Thus, as derived in reference 4

$$\text{Pitching moment} = M = C_m \frac{1}{2} \rho V^2 Ad \tag{8}$$

where C_m is a nondimensional pitching-moment coefficient.

Since the dynamic pressure is

$$Q = \frac{1}{2} \rho V^2 \tag{9}$$

it follows that

$$C_m = \frac{M}{QAd} \tag{10}$$

Dividing equation (6) by QAd gives

$$\left(\frac{I}{QAd} - \frac{\partial C_m}{\partial \ddot{\theta}}\right)\ddot{\theta} + \left(\frac{C}{QAd} - \frac{\partial C_m}{\partial \dot{\theta}}\right)\dot{\theta} + \left(\frac{K}{QAd} - \frac{\partial C_m}{\partial \theta}\right)\theta = \frac{M}{QAd} e^{i\omega t} \tag{11}$$

Thus, by using the characteristic time $\frac{d}{V}$ to nondimensionalize the derivatives of θ, by definition

$$\left.\begin{aligned} C_{m_{\ddot{\theta}}} &= \frac{\partial C_m}{\partial\left(\frac{\ddot{\theta} d^2}{V^2}\right)} \\ C_{m_{\dot{\theta}}} &= \frac{\partial C_m}{\partial\left(\frac{\dot{\theta} d}{V}\right)} \\ C_{m_\theta} &= \frac{\partial C_m}{\partial \theta} \end{aligned}\right\} \tag{12}$$

From equations (12) it follows that

$$\left.\begin{aligned} \frac{\partial C_m}{\partial \ddot{\theta}} &= \frac{d^2}{V^2} C_{m_{\ddot{\theta}}} \\ \frac{\partial C_m}{\partial \dot{\theta}} &= \frac{d}{V} C_{m_{\dot{\theta}}} \\ \frac{\partial C_m}{\partial \theta} &= C_{m_\theta} \end{aligned}\right\} \tag{13}$$

Substitution of equations (13) into equation (11) gives the desired differential equation of motion.

$$\left(\frac{I}{QAd} - \frac{d^2}{V^2} C_{m_{\ddot{\theta}}}\right)\ddot{\theta} + \left(\frac{C}{QAd} - \frac{d}{V} C_{m_{\dot{\theta}}}\right)\dot{\theta} + \left(\frac{K}{QAd} - C_{m_\theta}\right)\theta = \frac{M}{QAd} e^{i\omega t} \tag{14}$$

It is apparent from the left-hand side of equation (14) that C_{m_θ} is the aerodynamic equivalent of K and that at a trim angle of attack a negative value of C_{m_θ} would indicate that the rigid body has static stability in pitch about that trim angle of attack. At angles of attack other than those of trim, the value of C_{m_θ} indicates the local slope of the static pitching-moment curve. Likewise, $C_{m_{\dot\theta}}$ is the aerodynamic equivalent of C and a negative value of $C_{m_{\dot\theta}}$ would indicate that the rigid body has positive aerodynamic damping in pitch. $C_{m_{\ddot\theta}}$ is the aerodynamic equivalent of I and a negative value of $C_{m_{\ddot\theta}}$ would indicate that the rigid body has positive aerodynamic inertia in pitch.

1.3 Solution of the Differential Equation of Motion

The complete solution to equations such as equation (14) consists of two parts. The first part is obtained by solving equation (14) when the term representing the forcing function is deleted. This transient solution describes the free motion of the model system in the absence of the forcing function. The second part is any solution of the nonhomogeneous equation. This steady-state solution describes the response of the system to the forcing function and the behavior which it represents is called the forced motion.

In the small-amplitude forced-oscillation technique of dynamic-stability testing, the existence of the transient solution is never allowed because both the frequency and the amplitude of the motion are rigidly controlled such that at all times the complete "solution" is known to be the forced steady-state solution

$$\theta = \Theta e^{i(\omega t-\eta)} \tag{15}$$

where η is the phase angle between the applied moment of the forcing function, M, and the resulting angular displacement of amplitude Θ. The actual unknowns of the differential equation are the coefficients which can be determined if M, Θ, η, and ω are known. From equation (15) it follows that

$$\left.\begin{aligned} \dot{\theta} &= i\omega\Theta e^{i(\omega t-\eta)} \\ \ddot{\theta} &= -\omega^2\Theta e^{i(\omega t-\eta)} \end{aligned}\right\} \tag{16}$$

Substitution of equations (15) and (16) into equation (14) and dividing by $\Theta e^{i(\omega t-\eta)}$ gives the algebraic equation

$$-\omega^2\left(\frac{I}{QAd} - \frac{d^2}{V^2} C_{m_{\ddot{\theta}}}\right) + i\omega\left(\frac{C}{QAd} - \frac{d}{V} C_{m_{\dot{\theta}}}\right) + \left(\frac{K}{QAd} - C_{m_\theta}\right) = \frac{M}{QAd\Theta} e^{i\eta} \tag{17}$$

By using the Euler identity

$$e^{i\eta} = \cos \eta + i \sin \eta$$

it is a simple matter to equate the in-phase and quadrature components of equation (17).

Equating the in-phase-with-displacement components gives

$$\left(\frac{K}{QAd} - C_{m_\theta}\right) - \omega^2\left(\frac{I}{QAd} - \frac{d^2}{V^2} C_{m_{\ddot{\theta}}}\right) = \frac{M \cos \eta}{QAd\ \Theta} \tag{18}$$

and equating the quadrature components gives

$$\omega\left(\frac{C}{QAd} - \frac{d}{V} C_{m_{\dot\theta}}\right) = \frac{M \sin \eta}{QAd\Theta} \tag{19}$$

Solving equations (18) and (19) for the nondimensional aerodynamic parameters gives

$$C_{m_\theta} - \left(\frac{\omega d}{V}\right)^2 C_{m_{\ddot\theta}} = - \frac{M \cos \eta}{QAd\Theta} + \frac{(K - I\omega^2)_{mech}}{QAd} \tag{20}$$

$$C_{m_{\dot\theta}} = \frac{V}{d}\left(- \frac{M \sin \eta}{QAd\Theta\omega} + \frac{C_{mech}}{QAd}\right) \tag{21}$$

where the mechanical characteristics are now explicitly identified by the addition of the subscript "mech."

In order to take mechanical or tare values into account, a distinction is made between wind-on and wind-off data. Thus, for wind-on measurements equations (20) and (21) may be written

$$C_{m_\theta} - \left(\frac{\omega d}{V}\right)^2 C_{m_{\ddot\theta}} = - \left(\frac{M \cos \eta}{QAd\Theta}\right)_{\text{wind on}} + \frac{(K - I\omega^2)_{mech}}{QAd} \tag{22}$$

and

$$C_{m_{\dot\theta}} = \frac{V}{d}\left[- \left(\frac{M \sin \eta}{QAd\Theta\omega}\right)_{\substack{\text{wind}\\ \text{on}}} + \frac{C_{mech}}{QAd}\right] \tag{23}$$

In order to determine the mechanical properties of the system, wind-off measurements are made. From equations (20) and (21) it follows that when the aerodynamic terms are zero (wind off) the mechanical properties of the system are

$$(K - I\omega^2)_{mech} = \left(\frac{M \cos \eta}{\Theta}\right)_{wind\ off} \tag{24}$$

and

$$C_{mech} = \left(\frac{M \sin \eta}{\Theta\omega}\right)_{wind\ off} \tag{25}$$

Substitution of equation (24) into equation (22) and of equation (25) into equation (23) gives the desired expression for the aerodynamic characteristics of the model in terms of measurable quantities.

1.4 Nondimensional Stability Parameters

Thus the oscillatory-longitudinal-stability parameter is

$$C_{m_\theta} - \left(\frac{\omega d}{V}\right)^2 C_{m_{\ddot{\theta}}} = -\frac{1}{QAd}\left[\left(\frac{M \cos \eta}{\Theta}\right)_{wind\ on} - \left(\frac{M \cos \eta}{\Theta}\right)_{wind\ off}\right] \tag{26}$$

and the damping-in-pitch parameter is

$$C_{m_{\dot{\theta}}} = -\frac{V}{QAd^2}\left[\left(\frac{M \sin \eta}{\omega\Theta}\right)_{wind\ on} - \left(\frac{M \sin \eta}{\omega\Theta}\right)_{wind\ off}\right] \tag{27}$$

The values of A and d are related to the geometry of the body being tested and are measurable by direct means. The equations used to determine the values of V and Q are found in reference 5. Thus, in order to determine $C_{m_\theta} - \left(\frac{\omega d}{V}\right)^2 C_{m_{\ddot{\theta}}}$ and $C_{m_{\dot{\theta}}}$ it is necessary to measure wind-on and wind-off values of M, Θ, η, ω.

Noting that the wind-on measurements give the sum of the aerodynamic and mechanical characteristics, the wind-on terms may be written as

$$\left(\frac{M \cos \eta}{\theta}\right)_{\text{wind on}} = (K - I\omega^2)_{\text{aero}} + (K - I\omega^2)_{\text{mech}} \tag{28}$$

and

$$\left(\frac{M \sin \eta}{\omega\theta}\right)_{\text{wind on}} = C_{\text{aero}} + C_{\text{mech}} \tag{29}$$

By using equations (24), (25), (28), and (29) in equations (26) and (27) it follows that the oscillatory-longitudinal-stability parameter is

$$C_{m_\theta} - \left(\frac{\omega d}{V}\right)^2 C_{m_{\ddot{\theta}}} = - \frac{1}{QAd}(K - I\omega^2)_{\text{aero}} \tag{30}$$

and the damping-in-pitch parameter is

$$C_{m_{\dot{\theta}}} = - \frac{V}{QAd^2} C_{\text{aero}} \tag{31}$$

This form of the equations makes clear the association between the nondimensional aerodynamic parameters and the aerodynamic characteristics C_{aero} and $(K - I\omega^2)_{\text{aero}}$.

CHAPTER II

METHOD OF TEST

2.1 Mechanical Equipment

This section gives a general description of the mechanical equipment used in the test under the headings of wind tunnels and oscillation mechanism.

2.11 Wind Tunnels

Three wind tunnels were used to obtain the data presented herein. Common to all the tunnels was the ability to control relative humidity and total temperature of the air in the tunnel to prevent condensation shocks.

The data from a Mach number M of 0.20 to 1.20 were obtained in the Langley 8-foot transonic pressure tunnel (8-ft TPT). This single-return tunnel has a test section about 8 feet square and 5 feet long with slotted floor and ceiling to permit continuous operation from low subsonic speeds to a Mach number of about 1.20. The angle-of-attack mechanism maintains the model near the tunnel center line and has a range from about -4° to 14° when used in conjunction with the oscillation-balance mechanism.

The data at $M = 2.00$ and $M = 4.63$ were obtained in test sections 1 and 2, respectively, of the Langley Unitary Plan wind tunnel (UPWT).

Each of these single-return tunnels has a test section about 4 feet square and 7 feet long. Asymmetric sliding blocks can be used to change the Mach number from about 1.47 to 2.87 in test section 1 and from about 2.30 to 4.65 in test section 2. The angle-of-attack mechanism has a total range of about 25° when used in conjunction with the oscillation mechanism. The exact angles of attack obtained depend upon the relative orientation of the oscillation mechanism and the angle-of-attack mechanism.

2.12 Oscillation-Balance Mechanism

Exploded and assembled views of the forward portion of the oscillation-balance mechanism are presented as figure 1. The oscillation-balance mechanism consists of a strain-gage balance which is rigidly forced to perform a single-degree-of-freedom angular oscillation. The rotary motion of an amplidyne controlled d-c motor is used to give the essentially sinusoidal oscillatory motion to the balance through a crank and Scotch-yoke mechanism. The frequency of oscillation can be varied from near 0 to about 25 cycles per second. A mechanical spring is mounted inside the oscillation balance in such a way that the model being tested is connected to ground (the supporting sting) through the spring as well as through the moment sensing strain-gage beams of the oscillation balance. The mechanical spring has mounted to it a wire strain-gage bridge which provides an output voltage proportional to model displacement with respect to the fixed sting.

2.2 Measurements

Developed in detail in chapter I are the equations for the oscillatory-longitudinal-stability parameter (eq. (26)) and the damping-in-pitch parameter (eq. (27)). As pointed out in chapter I, in order to determine these parameters it is necessary to know the wind-on and wind-off values of M, θ, η, and ω. A block diagram of the electronic circuits which are used to determine M, θ, η, and ω is presented in figure 2(a). Also shown in figure 2(a) are the mathematical representations of the signals at each stage in both the M and θ circuits. Where necessary, details of the various components will be given in the sections which follow.

2.21 Determination of M

As shown in figure 2(a), the 3-kilocycle voltage source supplies 2.5 volts rms to two semiconductor four-arm strain-gage bridges located on beam elements of the oscillation balance. (For simplicity, the two bridges are shown in figure 2 as a single moment bridge.) The bridges are physically forward of the oscillation axis of the balance and are positioned in such a way that one bridge is primarily sensitive to pitching moments and the other bridge is primarily sensitive to normal forces. The outputs of the two bridges are combined at the oscillation balance in such a manner that any moment with respect to the oscillation axis which is applied to the balance produces an output voltage which is directly proportional to the applied moment. Thus, the oscillatory moment of the forcing function modulates the 3-kilocycle carrier voltage at the frequency of oscillation of the model system. The modulated signal from the bridges is then amplified by a constant-gain linear amplifier and passed through an induction resolver which is rotating at the frequency of oscillation of the model system. (The induction resolver is essentially a transformer with rotary variable coupling between primary and secondary windings. The windings are distributed in the various stator and rotor slots in such a manner as to obtain a true sinusoidal transformation ratio. The transformation ratios of the two secondary windings differ in phase by $\frac{\pi}{2}$ with respect to either primary winding as the rotor is turned.) The resolver resolves the input signal into orthogonal components which are demodulated by phase-sensitive demodulators. The resulting signals are filtered and read on digital voltmeters. The resolver-filter-voltmeter system shown in figure 2(a) performs the very important function of acting as an extremely narrow band-pass filter and completely eliminates the effects of random moments due to air-stream turbulence or other causes. The unique feature of this type of filter is that the center frequency of the band is always the frequency of oscillation of the model system. The principles involved are explained in detail in references 6 and 7. The voltmeter readings are multiplied by the factors necessary to account for sensitivity and amplifier attenuation settings and the value of M is determined from the resulting orthogonal components referenced to the rotor position of the moment resolver.

The determination of the sensitivities is accomplished by producing a known unbalance of the strain-gage bridges by using a resistor which can be inserted across one arm of the bridge. Figure 2(b) shows the moment circuit in block diagram form with the mathematical representation of the signals at each stage which would be present during the determination of the sensitivity constant for the M_r portion of the circuit. The other sensitivities are determined in the same manner.

2.22 Determination of Θ

As can be seen in figure 2(a), the electronic circuitry used to determine the amplitude of the angular displacement Θ is identical to that which is used to determine M with the exception that 10 volts rms are applied to a single four-arm wire strain-gage bridge. As was noted in 2.12, the displacement bridge is located on the mechanical spring of the oscillation balance and gives an output directly proportional to angular displacement of the oscillation balance with respect to the supporting sting. The value of Θ is determined from the orthogonal components of Θ referenced to the rotor position of the displacement resolver.

2.23 Determination of η

The M and Θ resolvers are physically alined so that the components of M and Θ are, in effect, referred to a common reference axis system. The angle between M and the reference r axis is determined from the orthogonal components M_i and M_r.

$$\zeta = \tan^{-1}\left(\frac{M_i}{M_r}\right)$$

and the angle between Θ and the reference r axis is determined from the orthogonal components Θ_i and Θ_r.

$$\xi = \tan^{-1}\left(\frac{\theta_i}{\theta_r}\right)$$

The desired phase angle is thus $\eta = \zeta - \xi$.

2.24 Determination of ω

As shown in figure 2(a), there is fastened to the shaft of one of the resolvers a 100-tooth gear which, in conjunction with an induction coil pick-up, is used to generate 100 pulses per cycle. The pulses are amplified, limited, and sent to an electronic counter where the number of pulses per second is counted. Because the least count of this system is one pulse per cycle, the accuracy increases with increasing frequency. For example, at 4 cps, frequency is determined to about one part in 400 and at 10 cps, frequency is determined to about one part in 1000.

CHAPTER III

TESTS OF SPHERE

3.1 Test Sphere

The design dimensions of the test sphere are given in figure 3 and a photograph of the test sphere installed on the oscillation-balance mechanism is presented as figure 4. The sphere was made of glass-fiber cloth and plastic and was secured to the oscillation-balance mechanism by means of an aluminum adapter. The three oscillation centers shown in figure 3 were obtained by using adapters of different lengths. The test sphere has a wall thickness of about 0.20 inch and is sufficiently rigid to prevent significant deformations due to aerodynamic or inertia loads. The base opening in the sphere necessary for sting clearance is also shown in figure 3.

Three-dimensional roughness in the form of sparsely distributed grains of No. 60 corborundum, which has a nominal height of 0.0117 inch (about 300 microns), was applied in a 1/8-inch wide band to the sphere for one test of configuration 2 at $M = 2.00$. The location of the roughness is shown in figure 3.

3.2 Test Conditions

Details of the test values of Mach number, Reynolds number, reduced-frequency parameter, and mean angle of attack for the three configurations tested may be obtained from the plotted data and keys of figure 5.

A constant free-stream Reynolds number of about 2×10^6, based on the diameter of the sphere, was maintained throughout the test except at the lowest test Mach number of 0.20. At $M = 0.20$ it was possible to get both a subcritical Reynolds number of 0.27×10^6 and a supercritical Reynolds number of 1.00×10^6.

The three-dimensional roughness described in section 3.1 was added to the sphere to insure a turbulent boundary layer forward of the location of flow separation. The size and location of the roughness was determined by the method of reference 8.

All data were taken at the frequency of velocity resonance for the oscillating system except at $M = 0.75$ where some additional data were taken at about twice and one-half the frequency of velocity resonance at $\alpha = 0^{\circ}$.

Tunnel total temperature was varied from 100° F to 110° F in the 8-ft TPT depending on Mach number and was held constant at 125° F and 175° F in UPWT test section 1 and UPWT test section 2, respectively. Dynamic pressure was varied from 14.4 psf at $M = 0.20$ to 568 psf at $M = 2.00$. The speed of the airflow varied from 231 ft/sec at $M = 0.20$ to about 2487 ft/sec at $M = 4.63$.

The amplitude of the forced oscillation was approximately 2°, ranging from 1.89° to 2.05°. (The range in oscillation amplitude for the sphere was to a large extent the result of excessive clearance due to wear between the crank and Scotch-yoke shown in figure 1. The smaller amplitudes occur just below the frequency for velocity resonance whereas the larger amplitudes occur just above the frequency for velocity resonance where the inertia force overcomes the spring force and allows the oscillating system to "fan out" to the extent allowed by any clearance between the crank and Scotch-yoke. Because the oscillating system was usually being operated very near the frequency for velocity resonance, the motion of the sphere remained essentially sinusoidal. Although unpublished data have shown that changing the amplitude of oscillation from 2° to 1° can have an effect on the data, these effects were only observed in regions where C_m changed very rapidly with α. The effect is clearly one of averaging the nonlinear aerodynamic characteristics over different ranges of α. Since the change in C_m with α for any of the sphere configurations is gradual, it is believed that the slight variation in amplitude had no effect on the data presented herein.)

3.3 Corrections

3.31 Flow Angularity

The values of mean angle of attack have been corrected for flow angularity in the test section. The corrections apply strictly only for a model at the vertical center of the wind tunnel, however, inasmuch as the data near $\alpha = 0^{\circ}$ is of primary interest and the $\alpha = 0^{\circ}$ data were taken near the center of the wind tunnel, a constant value of flow angularity was applied to all of the data as a first-order correction to the measured mean angle of attack.

3.32 Tunnel Constraints

No corrections for tunnel constraints have been applied. The effect of the tunnel walls are assumed to be small and are neglected. The effect of the supporting sting was not investigated but is assumed to be small and no corrections have been applied. Further comments concerning sting-interference effects are made in section 4.1.

3.33 Tare Values

The determination of wind-off or tare characteristics is discussed in appendix I. Because the mechanical spring of the system was used for a number of wind-tunnel tests in addition to the testing of the sphere, it was possible to get an accurate value for K_{mech}. The average value of K_{mech} as determined from 102 sets of tare data (consisting of over 600 datum points) was 38.6 ft-lb/rad with a probable error of ±1.1 ft-lb/rad. The rather large magnitude of the probable error has subsequently been traced to a random zero shift in the output of the moment bridge with changing temperature. A zero shift in itself has no direct effect on the data obtained while the balance is being oscillated, however, because the sensitivity of the circuits are determined statically, the random static zero shift resulted in considerable scatter in the sensitivity constants which have a direct effect on the data.

The average value of ω^2 for wind-off velocity resonance for a given configuration was divided into the average value of K_{mech} to determine I_{mech} for the different configurations. (Because the method of operation dictates that ω^2 for velocity resonance is determined by nulling the in-phase-with-displacement component of the moment signal, the sensitivity of the moment balance has no first-order effect on the determination of ω^2 for velocity resonance.)

As pointed out in appendix I, the value of C_{mech} was determined at the frequency of wind-off velocity resonance for each configuration and applied as a correction to the wind-on data. The tare values of C were generally at least an order of magnitude smaller than the wind-on values of C except for configuration 2 at the 8-foot TPT where the small values of wind-on damping coefficients were often of the same magnitude as the tare values of the damping coefficient.

3.4 Presentation of Results

The damping-in-pitch parameter $C_{m_{\dot{\theta}}}$ and the oscillatory-longitudinal-stability parameter $C_{m_{\theta}} - \left(\frac{\omega d}{V}\right)^2 C_{m_{\ddot{\theta}}}$ are presented graphically in figure 5 as functions of mean angle of attack α for the various Mach numbers.

CHAPTER IV

DISCUSSION OF RESULTS

4.1 Oscillatory-Longitudinal-Stability Parameter

The oscillatory-longitudinal-stability parameter gives the average slope of the oscillatory-pitching-moment-with-angle-of-attack curve over the angle-of-attack range from $\alpha - \Theta$ to $\alpha + \Theta$, where Θ is the amplitude of the forced oscillation. A negative value of this parameter at a trim angle of attack indicates that the sphere is dynamically stable with respect to that trim angle of attack.

Referring again to figure 3, it is seen that the oscillation centers for configurations 1, 2, and 3 are respectively forward of, coincident with, and rearward of the geometric center of the sphere. Static pitching-moment data were not obtained for the three configurations, however, from symmetry considerations it is clear that if the flow conditions over the sphere were symmetrical C_m would be zero for all three configurations at $\alpha = 0^{\circ}$ and therefore $\alpha = 0^{\circ}$ would be a trim angle of attack for the three configurations. Assuming that only symmetrical drag forces are acting on the sphere as angle of attack is varied, it would also be expected that at the static trim position at $\alpha = 0^{\circ}$ configurations 1, 2, and 3 would exhibit respectively positive, neutral, and negative static stability in pitch. (Positive static stability in pitch at a static trim position is indicated by a negative value of the static-longitudinal-stability coefficient C_{m_θ}.) As can be seen in figure 5, a progressive trend toward decreased oscillatory stability at $\alpha = 0^\circ$ is observed for configuration 1 as Mach number is decreased from $M = 2.00$ to $M = 0.58$. Some unexpected data were obtained at $\alpha = 0^\circ$, $M = 0.58$ where this apparently statically stable configuration exhibits pronounced oscillatory instability. Although these data have not been verified, this oscillatory instability indicates that possibly at the reduced frequency at which the data were taken, the aerodynamic-inertia term $C_{m_{\ddot\theta}}$ was dominant in the oscillatory-longitudinal-stability parameter $C_{m_\theta} - \left(\frac{\omega d}{V}\right)^2 C_{m_{\ddot\theta}}$. (A method by which the values of C_{m_θ} and $C_{m_{\ddot\theta}}$ may be obtained experimentally by using the small-amplitude forced-oscillation test technique is presented in appendix II.)

The nearly neutral oscillatory stability which was expected at $\alpha = 0^\circ$ for configuration 2 is seen at $M = 0.58$, 0.90, 1.00, 1.20, 2.00, and at the higher Reynolds number at $M = 0.20$. However, this configuration has oscillatory stability at the lower Reynolds number (subcritical) at $M = 0.20$ and oscillatory instability at $M = 4.63$. Anomalous results were obtained for both the damping and the oscillatory-stability data for this configuration at $M = 0.75$. Data at about twice and one-half the frequency of velocity resonance was obtained at $\alpha = 0^\circ$ when very erratic voltmeter readings were observed at the frequency of velocity resonance. Although there appears to be an effect of frequency of oscillation on the oscillatory-stability data, it is improbable that this is the case because (to the first order) there can be neither a C_{m_θ} nor a $C_{m_{\dot{\theta}}}$ term for this configuration with the oscillation and geometric centers coincident. This rather awkward looking data is probably the result of asymmetrical surface conditions on the sphere which caused asymmetrical flow and hence asymmetrical drag over the sphere. Some experimental verification that the anomalous results are due to asymmetrical flow can possibly be obtained from the limited fixed transition data for configuration 2 at $M = 2.00$ shown in figure 5(g). A positive value of the oscillatory-stability parameter was measured for the supposedly smooth sphere indicating asymmetrical flow whereas with fixed transition and therefore more symmetrical flow, the oscillatory-stability parameter was zero as would be expected.

At $M = 2.00$ the oscillatory-stability parameter of configuration 3 is a mirror image of the oscillatory-stability parameter of configuration 1. This expected equal and opposite relationship is seen to become somewhat more distorted as Mach number is decreased to $M = 1.20$ and $M = 1.00$. At $M = 0.58$ the trends in the oscillatory-stability parameters for these two configurations are similar for $\alpha = 0^{\circ}$ and diverge sharply at $\alpha = -4^{\circ}$. The slightly asymmetrical data obtained for this configuration at $M = 1.20$ and $M = 1.00$ are again believed to be the result of flow asymmetry over the sphere due to different degrees of surface roughness above and below the horizontal center line of the sphere. The results obtained at $\alpha = -4^{\circ}$, $M = 0.58$ indicate that with the thinner boundary layer which exists for this Mach number, the effects of surface asymmetry were sufficient to change completely and drastically the flow over the sphere. The possibility of asymmetrical sting interference effects does exist because the supporting sting used in the 8-ft TPT becomes slightly asymmetric in the pitch plane about 2 feet downstream of the oscillation axis. Asymmetrical forces being transmitted through the subsonic boundary layer of the sting was considered as a possible cause of the observed asymmetrical data. However, the fact that configuration 1 was 2 inches closer to the sting asymmetry than configuration 3 (due to the spacers mentioned in section 3.1) and that the data for configuration 1 was completely free of the asymmetry seen in the data for configuration 3, strongly suggests that the asymmetrical sting did not produce the asymmetrical data obtained for configuration 3. In addition, the data of reference 9 shows that the effects of sting size and length on cones with spherical-segment bases is very small for the sting-length-to-model-diameter and sting-diameter-to-model-diameter ratios which existed for the tests in both the 8-ft TPT and the UPWT. A definite explanation of the asymmetrical data must await further wind-tunnel tests.

4.2 Damping-in-pitch Parameter

The damping-in-pitch parameter is obtained from the average value of the damping coefficient of the sphere over the range of angle of attack from $\alpha - \theta$ to $\alpha + \theta$ where θ is, as before, the amplitude of the forced oscillation. A negative value of this parameter at any mean angle of attack indicates that the sphere experienced positive aerodynamic damping during the oscillations about the mean angle of attack.

The levels of damping for the three configurations do not differ as much as the levels in oscillatory stability. The changes in oscillatory stability with mean angle of attack are accompanied by changes in damping with mean angle of attack. As pointed out in reference 10, this reciprocal relationship is often observed between oscillatory stability and damping for high drag bodies. That these parameters change together is to be expected since both parameters arise from the same flow over the body.

The aerodynamic damping data for configuration 1 shows the same symmetry about $\alpha = 0^{\circ}$ as the corresponding oscillatory-stability data. Positive damping was measured at $\alpha = 0^{\circ}$ at all Mach numbers at which this configuration was tested.

The damping for configuration 2 is generally small except for the data at $M = 0.75$ which has previously been described as suspect due (probably) to asymmetrical surface conditions. No effect of Reynolds number is observed on the damping at $M = 0.20$ although, as previously mentioned, the lower Reynolds number resulted in slightly greater oscillatory stability. The addition of the three-dimensional roughness to configuration 2 at $M = 2.00$ is seen to have had little effect on the damping.

The damping data for configuration 3 shows the same degree of asymmetry about $\alpha = 0^{\circ}$ as the corresponding oscillatory-stability data. Except for positive damping at $M = 2.00$, this configuration exhibited negative damping at $\alpha = 0^{\circ}$ at all Mach numbers at which it was tested. The slight variation in oscillatory stability between the three data points at $\alpha = 0^{\circ}$, $M = 2.00$ is accompanied by a large variation in the damping. Again, the only known cause for this variation and asymmetry is the extreme sensitivity of the flow over the sphere to the surface condition of the sphere.

CHAPTER V

CONCLUDING REMARKS

The aerodynamic damping and oscillatory stability in pitch of a sphere at Mach numbers from 0.20 to 4.63 have been determined experimentally in wind tunnels by using a small-amplitude single-degree-of-freedom forced-oscillation test technique. Some details of the test technique are included for the benefit of other workers in the same field who may be interested. Nomenclature suited to this type of wind-tunnel test is introduced in the development of the equations which were used to reduce the measured aerodynamic characteristics to nondimensional form.

Tests were made at oscillation amplitudes of about 2° at oscillation centers forward of, coincident with, and rearward of the geometric center of the sphere.

The oscillatory stability at $\alpha = 0^{\circ}$ decreases with decreasing Mach number for the configuration with the oscillation center forward of the geometric center. The unexpected oscillatory instability of this configuration at $M = 0.58$ indicates that possibly at the reduced frequency at which the data were taken, the usually ignored aerodynamic-inertia term $C_{m_{\ddot{\theta}}}$ was dominant in the oscillatory-stability parameter $C_{m_{\theta}} - \left(\frac{\omega d}{V}\right)^2 C_{m_{\ddot{\theta}}}$. Additional tests should be made not only to verify the data obtained herein but also to determine, by using the method presented in appendix II, the values of both $C_{m_{\theta}}$ and $C_{m_{\ddot{\theta}}}$.

The expected oscillatory-stability and aerodynamic-damping characteristics were measured for the configurations with the oscillation centers coincident with and rearward of the geometric center of the sphere except for asymmetry in some of the data near $\alpha = 0^{\circ}$. The observed asymmetry is attributed to asymmetrical flow over the sphere due to asymmetrical surface conditions. The limited amount of fixed transition data obtained at $M = 2.00$ indicates the desirability of repeating these tests with three-dimensional roughness applied to the spheres in an attempt to insure symmetrical flow over the spheres.

NOTATION

Units

The foot-pound-second system of units is used herein, however, the experimental data are presented in nondimensional form.

Axes

All moments, displacements, velocities, accelerations, aerodynamic derivatives, and aerodynamic parameters are referred to body axes originating at the oscillation centers of the model as shown in figure 3.

Symbols

The symbols used herein are defined as follows:

A	reference area, ft^2
a	speed of sound, ft/sec
C	viscous-damping coefficient, ft-lb-sec/rad
d	reference length, ft
e	base of natural system of logarithms
f	frequency of oscillation, cycles/sec
I	moment-of-inertia coefficient, $ft\text{-}lb\text{-}sec^2/rad$
i	complex operator, $i = \sqrt{-1}$
K	spring-stiffness coefficient, ft-lb/rad
M	pitching moment, ft-lb

M	free-stream Mach number, $\frac{V}{a}$, nondimensional
q	angular velocity due to pitching in free flight, radians/sec
$\dot{q}$	angular acceleration due to pitching in free flight, $\frac{dq}{dt}$, radians/sec^2
Q	free-stream dynamic pressure, $1/2\ \rho V^2$, lb/ft^2
R	free-stream Reynolds number, $\rho Vd/\mu$, nondimensional
t	time, sec
V	speed of flow, ft/sec
α	mean angle of attack, deg or radians
$\dot{\alpha}$	$\frac{d\alpha}{dt}$, radians/sec
η	phase angle between the applied moment of the forcing function and the angular displacement of the model with respect to the sting, deg or radians
Θ	amplitude of the angular displacement of the model with respect to the sting (one-half of peak-to-peak value), radians
θ	instantaneous angular displacement of the model with respect to the sting, radians
$\dot{\theta}$	$\frac{d\theta}{dt}$, radians/sec
$\ddot{\theta}$	$\frac{d^2\theta}{dt^2}$, radians/sec^2
μ	absolute viscosity of air, lb-sec/ft^2
ρ	free-stream mass density of air, lb-sec^2/ft^4
ω	angular velocity, $2\pi f$, radians/sec
$\frac{\omega d}{V}$	reduced-frequency parameter, nondimensional
C_m	pitching-moment coefficient, $\frac{\text{Pitching moment}}{QAd}$, nondimensional

Nondimensional aerodynamic derivatives

The following nondimensional aerodynamic derivatives associated with pitching motion are in terms of radians.

$$C_{m_\alpha} = \frac{\partial C_m}{\partial \alpha} \qquad\qquad C_{m_\theta} = \frac{\partial C_m}{\partial \theta}$$

$$C_{m_{\dot\alpha}} = \frac{\partial C_m}{\partial\left(\frac{\dot\alpha d}{V}\right)} \qquad C_{m_q} = \frac{\partial C_m}{\partial\left(\frac{q d}{V}\right)} \qquad C_{m_{\dot\theta}} = \frac{\partial C_m}{\partial\left(\frac{\dot\theta d}{V}\right)}$$

$$C_{m_{\dot q}} = \frac{\partial C_m}{\partial\left(\frac{\dot q d^2}{V^2}\right)} \qquad C_{m_{\ddot\theta}} = \frac{\partial C_m}{\partial\left(\frac{\ddot\theta d^2}{V^2}\right)}$$

Conventional derivatives (C_{m_α}, $C_{m_{\dot\alpha}}$, C_{m_q}, $C_{m_{\dot q}}$)

Derivatives used herein (C_{m_θ}, $C_{m_{\dot\theta}}$, $C_{m_{\ddot\theta}}$)

Nondimensional aerodynamic parameters

The following nondimensional aerodynamic parameters associated with pitching motion are in terms of radians. The equation for the parameters used herein are developed in chapter I.

$C_{m_\alpha} - \left(\frac{\omega d}{V}\right)^2 C_{m_{\dot q}}$	conventional oscillatory-longitudinal-stability parameter
$C_{m_\theta} - \left(\frac{\omega d}{V}\right)^2 C_{m_{\ddot\theta}}$	oscillatory-longitudinal-stability parameter used herein
$C_{m_q} + C_{m_{\dot\alpha}}$	conventional damping-in-pitch parameter
$C_{m_{\dot\theta}}$	damping-in-pitch "parameter" used herein

Subscripts:

aero	aerodynamic characteristics
mech	mechanical characteristics
wind on	measurements made with $V \neq 0$
wind off	measurements made with $V = 0$

APPENDIX I

DETERMINATION OF WIND-OFF OR TARE CHARACTERISTICS

Several tests have shown that wind-off or tare values determined at reduced pressures do not differ significantly from tare values determined at atmospheric pressure. Consequently, the tare values are usually determined from measurements made at atmospheric pressure. (Extension of this practice to Mach numbers greater than about 5 may be unwise inasmuch as the aerodynamic-damping moments usually decrease with increasing Mach number. Thus, the very slight difference between tares determined at atmospheric pressure and at greatly reduced pressures may be significant in determining the value of the damping coefficient at hypersonic speeds where tare and wind-on values of damping may be of the same order of magnitude.)

$(K - I\omega^2)_{mech}$

Wind-on data are usually taken at the frequency of wind-on velocity resonance (forcing moment in-phase with velocity). It is therefore desirable to be able to determine $(K - I\omega^2)_{mech}$ for any frequency because the frequency of wind-on velocity resonance usually changes with the changing aerodynamic properties as Mach number and angle of attack are varied. This is best accomplished by obtaining wind-off measurements over a range of frequencies and plotting $\left(\frac{M \cos \eta}{\Theta}\right)_{\text{wind off}}$ as a function of ω^2.

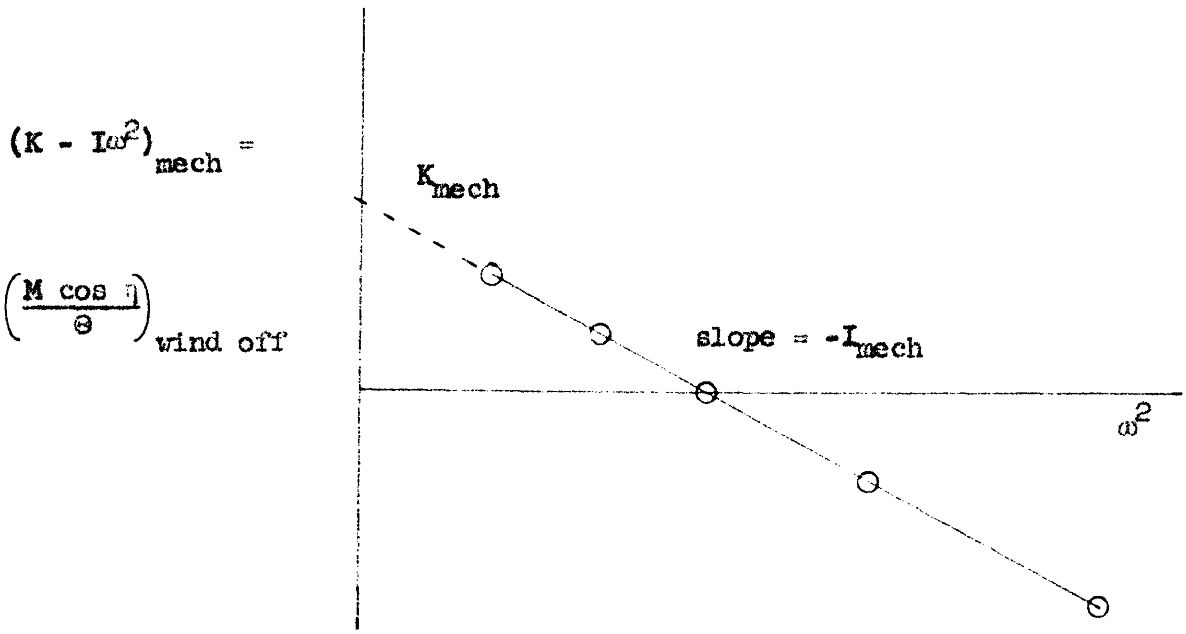

It can be seen from the sketch that the $\omega^2 = 0$ intercept of the resulting curve (obtained by extrapolation) gives the coefficient of the mechanical spring of the system K_{mech} and the slope of the curve gives the coefficient of the mechanical moment of inertia of the system I_{mech}.

It is possible to determine the proper value of $(K - I\omega^2)_{mech}$ to be used as the tare correction for any wind-on data point by multiplying I_{mech} by the value of ω^2 corresponding to the frequency of the wind-on data point and subtracting the result from K_{mech}. An additional advantage of this method is that possible random errors in the individual tare datum points are averaged out in the straight line fairing of the curve and are not likely to grossly influence the value of $(K - I\omega^2)_{mech}$ at any frequency.

C_{mech}

It has been shown in chapter I that for wind-off conditions, the mechanical damping coefficient is given by

$$C_{mech} = \frac{M \sin \eta}{\Theta\omega}$$

Due to a rather large probable error in determining η (about $\pm 2^{\circ}$) the greatest accuracy in determining the usually small value of C_{mech} is obtained when the variation of $\sin \eta$ with η is a minimum which is the case when the system is being operated at velocity resonance where, by definition, $\eta = \frac{\pi}{2}$ or $\frac{3\pi}{2}$. Because C_{mech} does not vary with frequency, the value of C_{mech} determined at wind-off velocity resonance is used as a tare correction for all of the wind-on data regardless of the frequency at which the individual wind-on datum points were obtained.

APPENDIX II

SEPARATION OF C_{m_θ} AND $C_{m_{\ddot{\theta}}}$

stability parameter $C_{m_\theta} - \left(\frac{\omega d}{V}\right)^2 C_{m_{\ddot{\theta}}}$ .nation as the oscillatory-longitudinal-stability parameter $C_{m_\theta} - \left(\frac{\omega d}{V}\right)^2 C_{m_{\ddot{\theta}}}$.

C_{m_θ} is the slope of the static-pitching-moment coefficient versus angle-of-attack curve and is the aerodynamic equivalent of a torsional-spring coefficient. Any variation of $C_{m_\theta} - \left(\frac{\omega d}{V}\right)^2 C_{m_{\ddot{\theta}}}$ from the value determined from static pitching-moment measurements is the effect of the inertia term $C_{m_{\ddot{\theta}}}$ because by definition C_{m_θ} is a static derivative.

The values of both C_{m_θ} and $C_{m_{\ddot{\theta}}}$ are determined by plotting the oscillatory-longitudinal-stability parameter as a function of $\left(\frac{\omega d}{V}\right)^2$. (Accurate values of the oscillatory-longitudinal-stability parameter can be obtained over a large range of reduced frequencies by using a sufficiently rigid small-amplitude forced-oscillation test technique.) The intercept of the resulting curve obtained by extrapolation to $\left(\frac{\omega d}{V}\right)^2 = 0$ is C_{m_θ}. The value of C_{m_θ} obtained in this manner is the slope of the pitching-moment-coefficient curve determined at the mean angle of attack of the model and is usually in good agreement with values of C_{m_θ} obtained from static pitching-moment measurements. The slope of the $C_{m_\theta} - \left(\frac{\omega d}{V}\right)^2 C_{m_{\ddot{\theta}}}$ versus $\left(\frac{\omega d}{V}\right)^2$ curve gives the desired value of $C_{m_{\ddot{\theta}}}$. The value of $C_{m_{\ddot{\theta}}}$ is usually small and is often neglected. Under certain conditions, however, the effect of $C_{m_{\ddot{\theta}}}$ on the oscillatory longitudinal stability may be very pronounced as the value of the reduced-frequency parameter, $\frac{\omega l}{V}$, is increased from zero.

REFERENCES

1. Duncan, W. J.: The Principles of the Control and Stability of Aircraft. Cambridge University Press, 1952.

2. Anon.: Fundamentals of Design of Piloted Aircraft Flight Control Systems, Volume II, Dynamics of the Airframe. BuAer Report AE-61-4, February 1953.

3. Thompson, J. S., and Fail, R. A.: Oscillatory Derivative Measurements on Sting-Mounted Wind-Tunnel Models: Method of Test and Results for Pitch and Yaw on a Cambered Ogee Wing at Mach Numbers up to 2.6. Royal Aircraft Establishment Report No. AERO 2668, July 1962.

4. Millikan, C. B.: Aerodynamics of the Airplane. John Wiley and Sons, Inc., [illegible].

5. Ames Research Staff: Equations, Tables, and Charts for Compressible Flow. NACA Report 1135, 1953.

6. Lessing, Henry C., Fryer, Thomas B., and Mead, Merrill H.: A System for Measuring the Dynamic Lateral Stability Derivatives in High-Speed Wind Tunnels. NACA TN 3348, December 1954.

7. Braslow, Albert L., Wiley, Harleth G., and Lee, Cullen Q.: A Rigidly Forced Oscillation System for Measuring Dynamic-Stability Parameters in Transonic and Supersonic Wind Tunnels. NASA TN D-1231, March 1962.

8. Tetervin, Neal: Theoretical Distribution of Laminar-Boundary-Layer Thickness, Boundary-Layer Reynolds Number and Stability Limit, and Roughness Reynolds Number for a Sphere and Disk in Incompressible Flow. NACA TN 4350, September 1958.

9. Wehrend, William R., Jr.: An Experimental Evaluation of Aerodynamic Damping Moments of Cones With Different Centers of Rotation. NASA TN D-1768, March 1963.

10. Kilgore, Robert A., and Barton, Richard L.: Wind-Tunnel Measurements of the Aerodynamic Damping and Oscillatory Stability in Pitch of Two High-Drag Bodies of Revolution at Mach Numbers From 0.60 to 1.20. NASA Proposed Paper.

VITA

Robert Ashworth Kilgore

Born in Coeburn, Virginia, October 25, 1932. Graduated from Clinchco High School in Clinchco, Virginia, May 1951; B.S., Emory and Henry College, May 1955.

The author has been an engineer at the Langley Research Center of the National Aeronautics and Space Administration since August 1957.

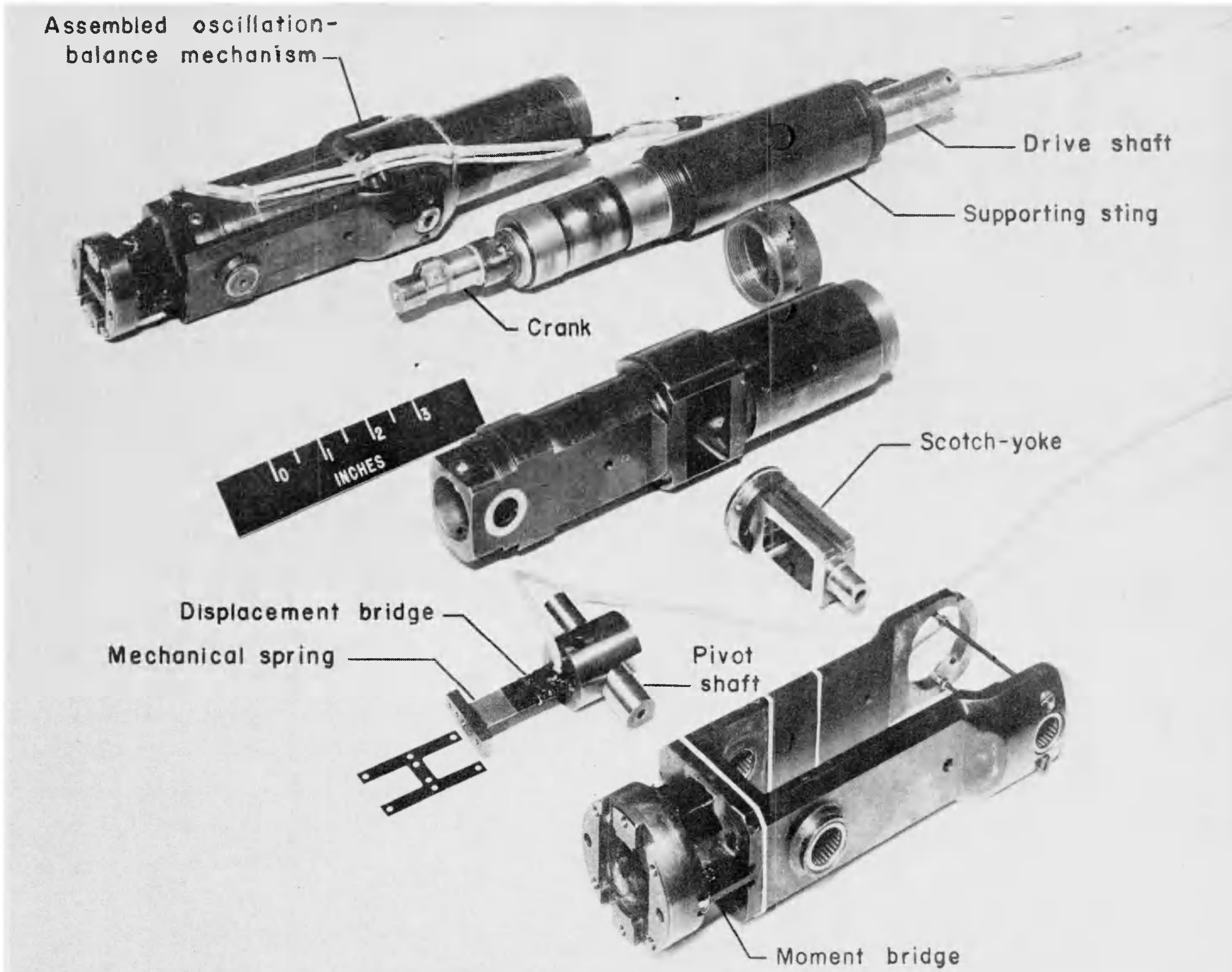

Figure 1.- Photograph of the forward portion of the oscillation-balance mechanism.

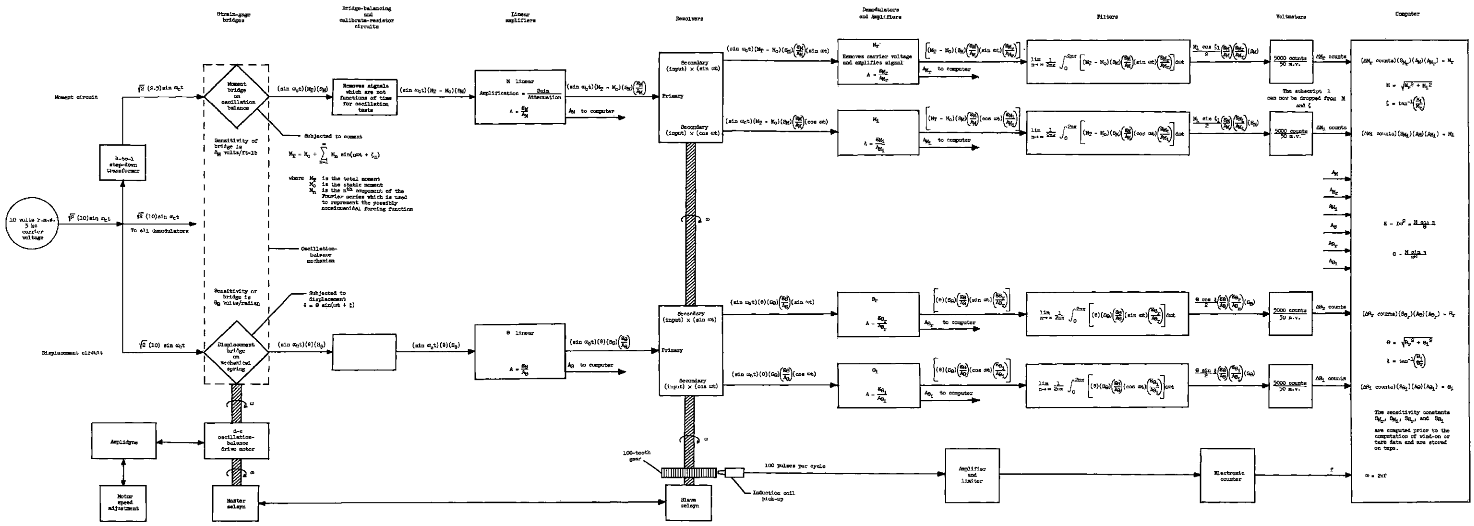

(a) Circuit used to determine M, Θ, η, and ω.

Figure 2.- Block diagram of electronic circuit.

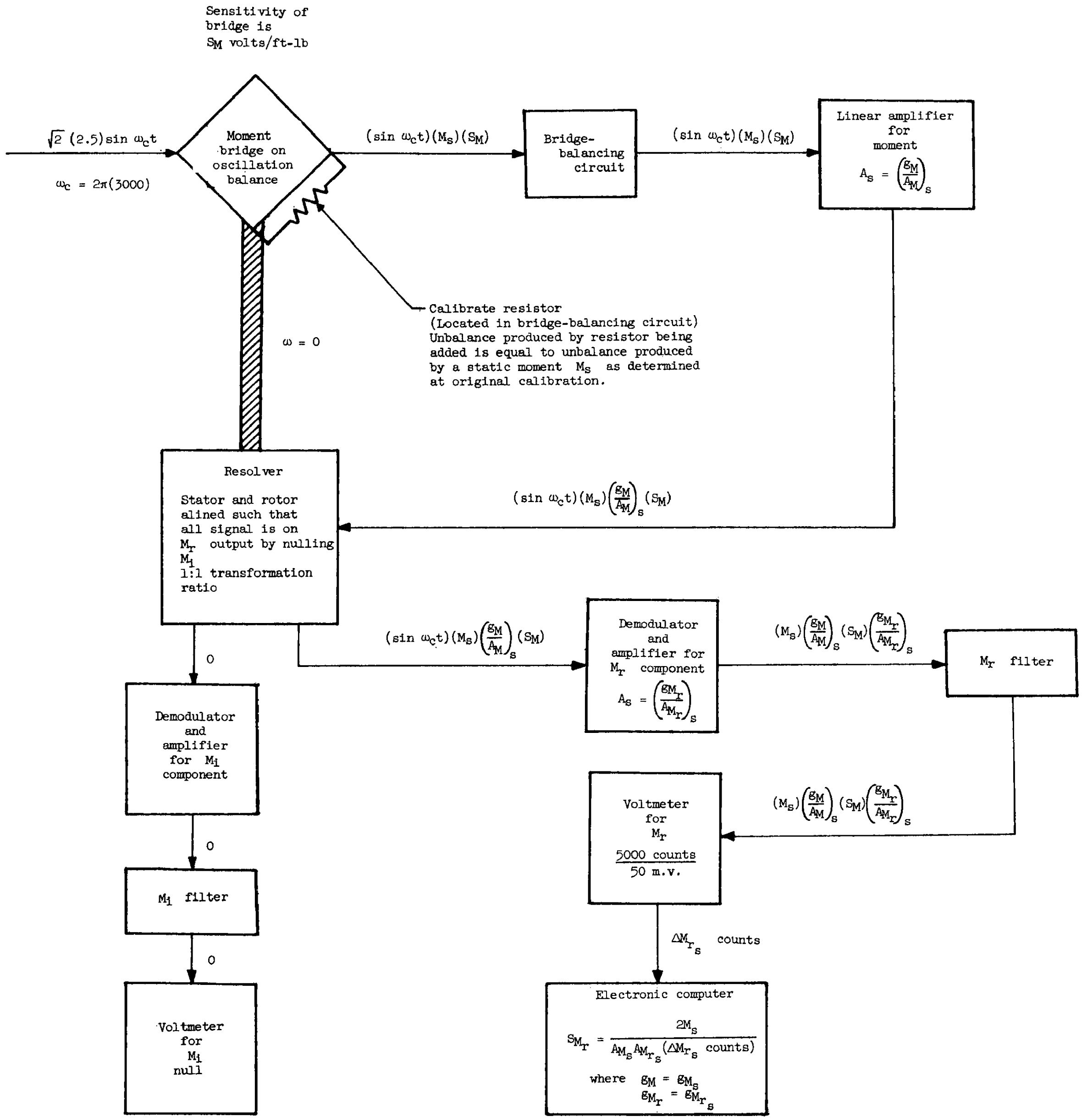

(b) Moment circuit during determination of sensitivity constant S_{M_r}.

Figure 2.- Concluded.

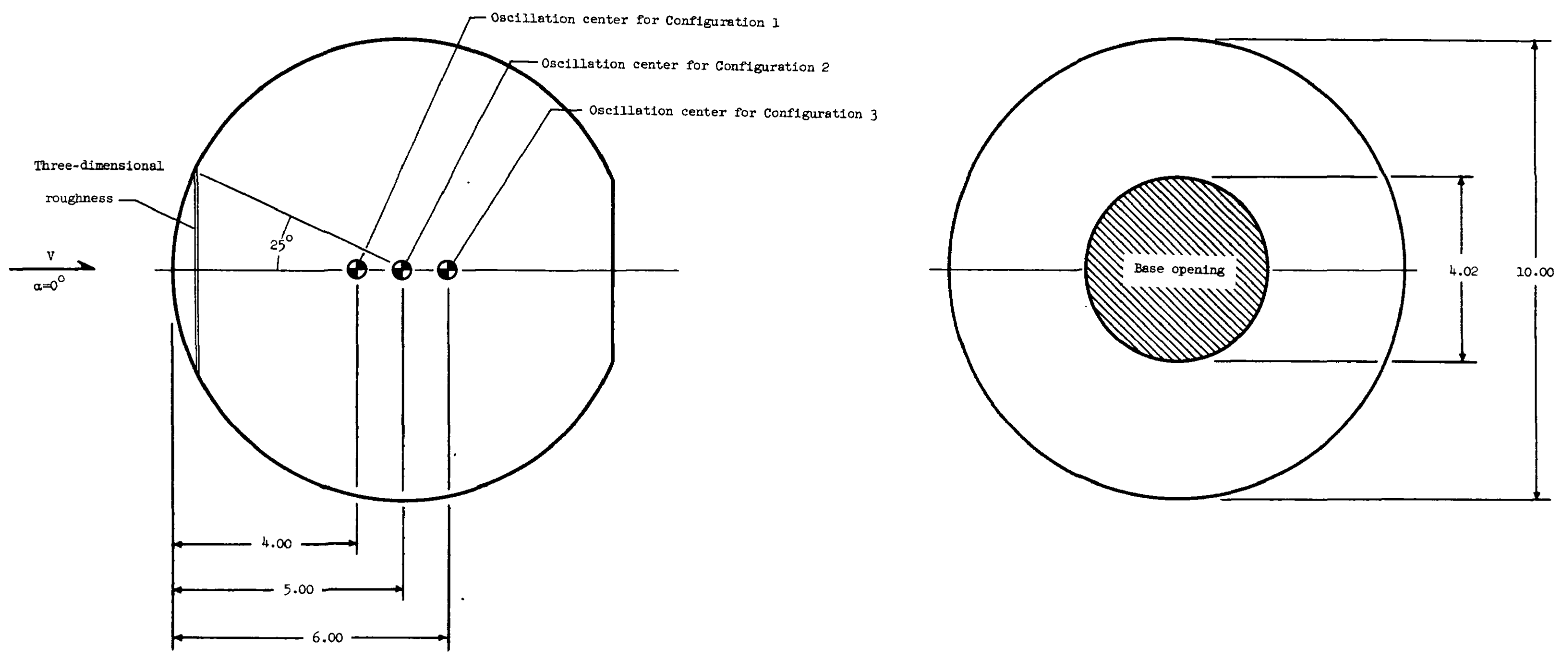

Figure 3.- Sketch of sphere showing design dimensions. All linear dimensions are in inches.

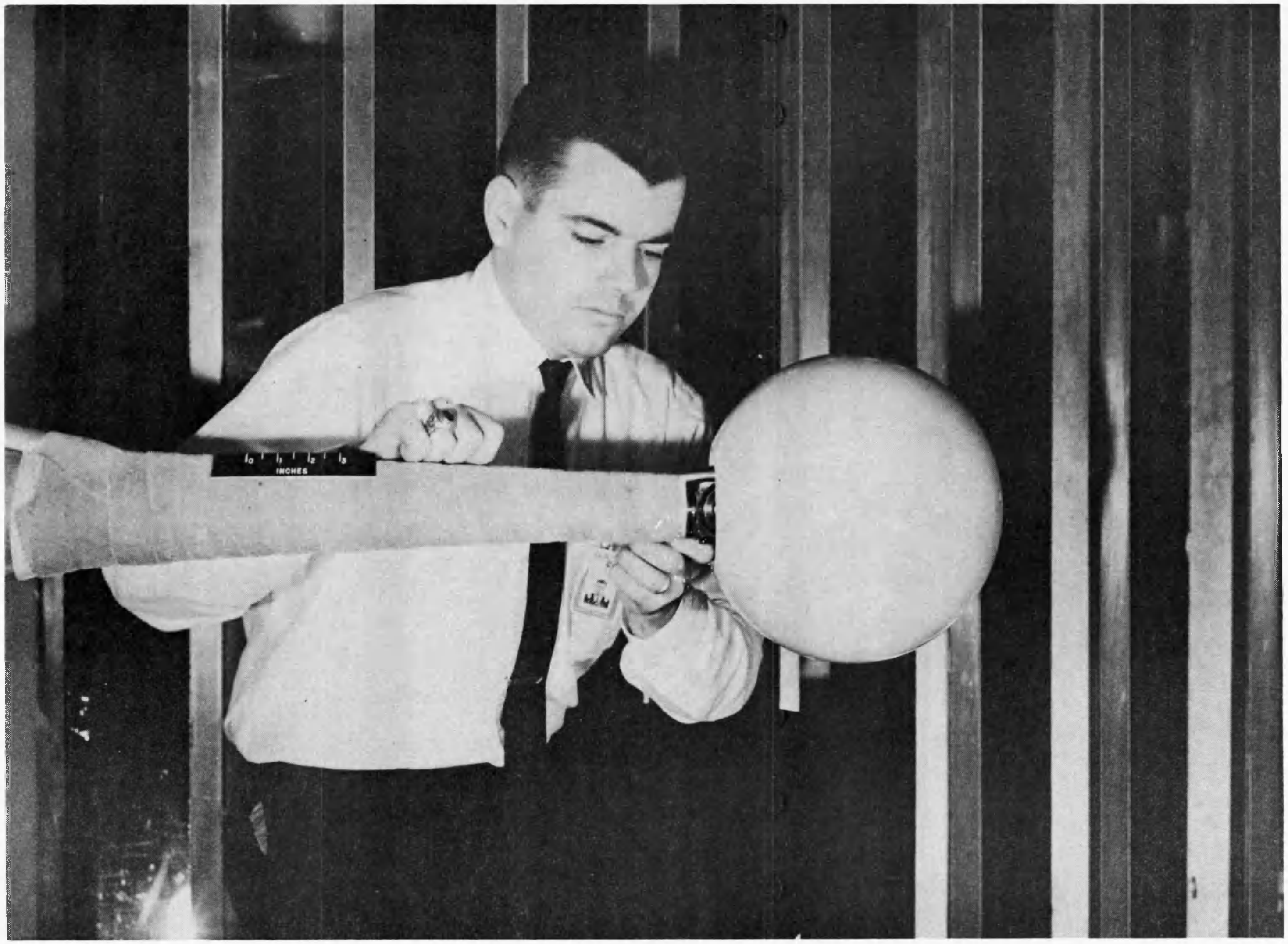

Figure 4.- Photograph of test sphere installed on oscillation-balance mechanism in test section 2 Langley Unitary Plan wind tunnel.

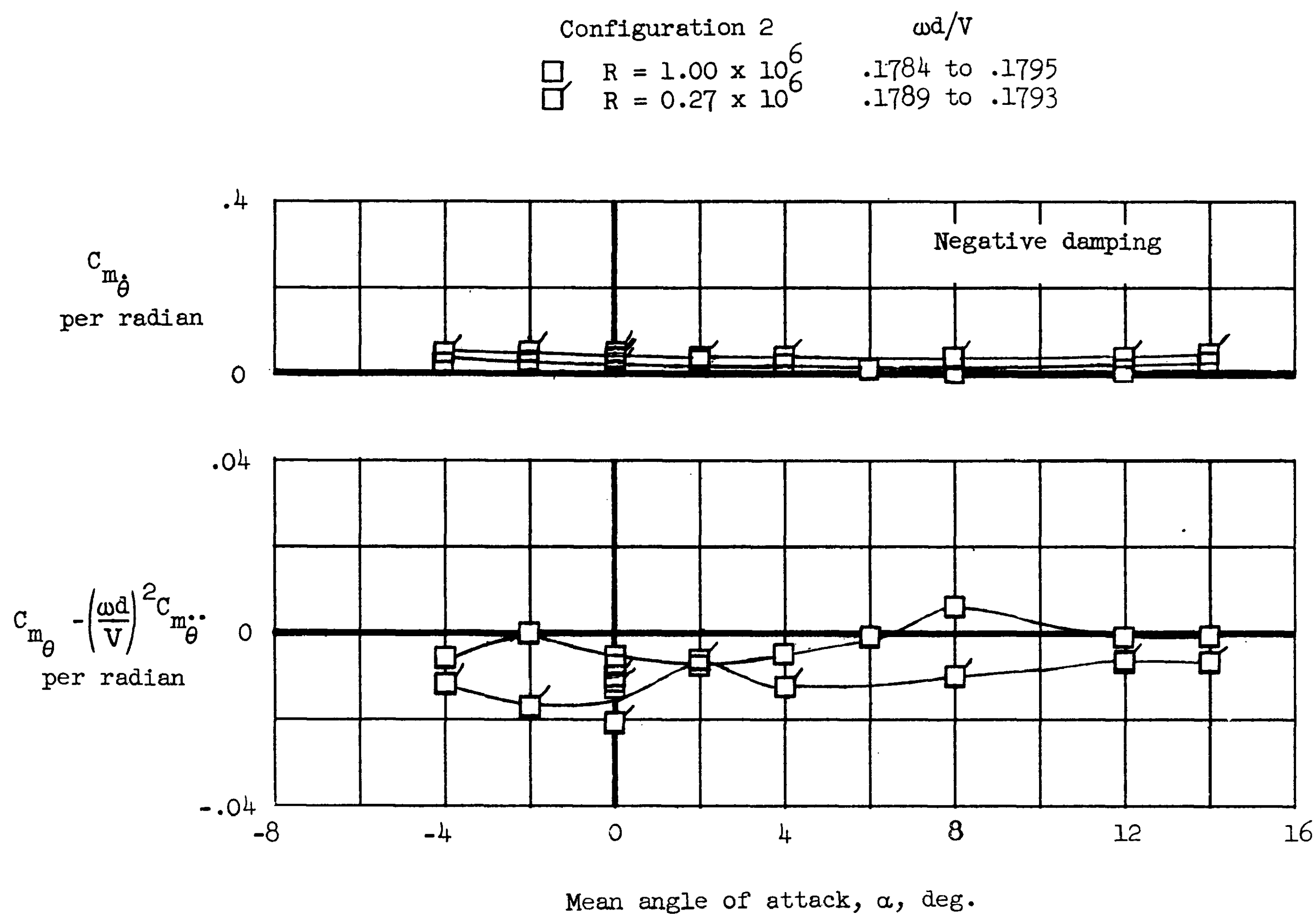

(a) M = 0.20.

Figure 5.- Variation of damping-in-pitch parameter and oscillatory-longitudinal-stability parameter with mean angle of attack. Free-stream Reynolds number was 2.00×10^6 except as noted.

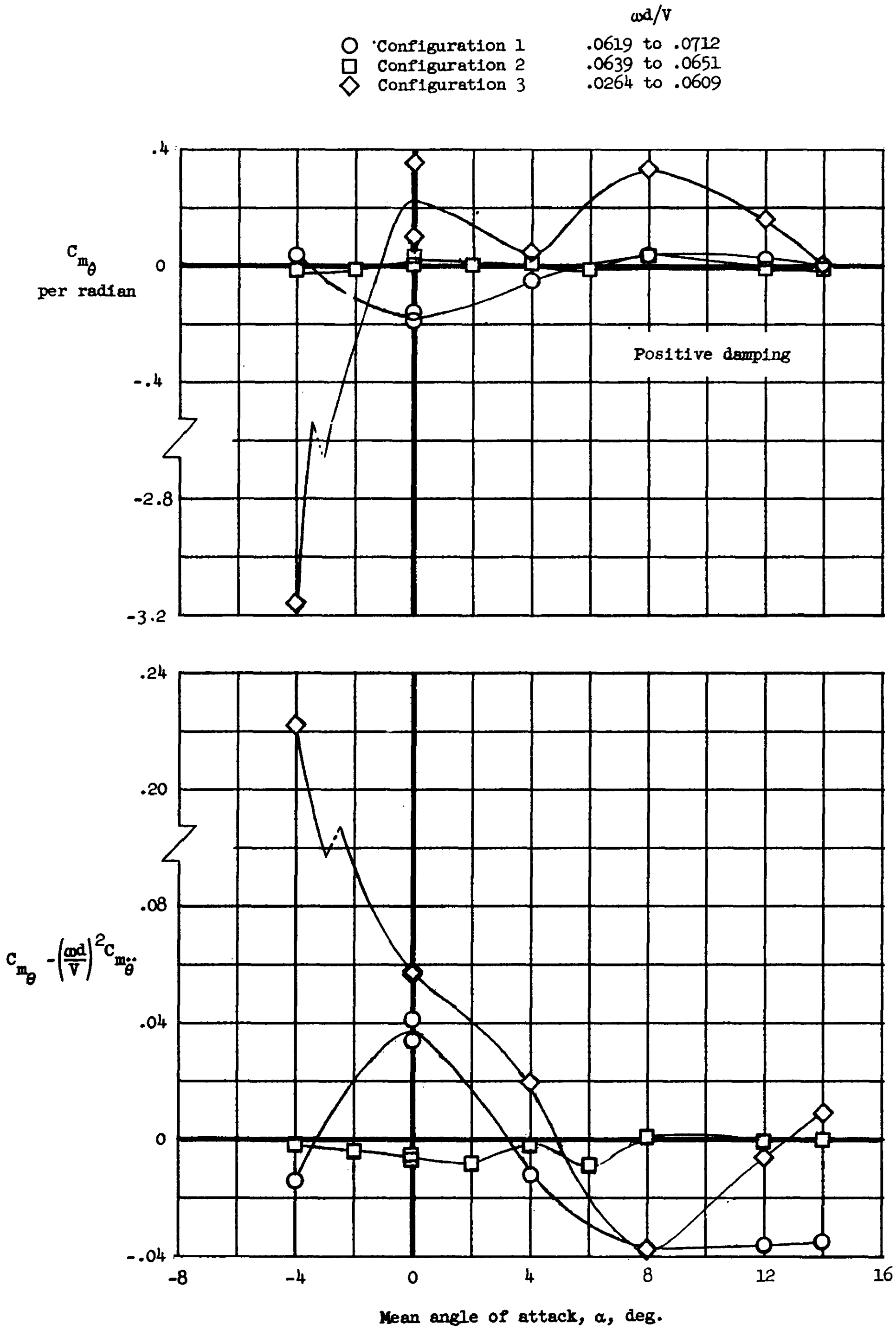

(b) M = 0.58.

Figure 5.- Continued.

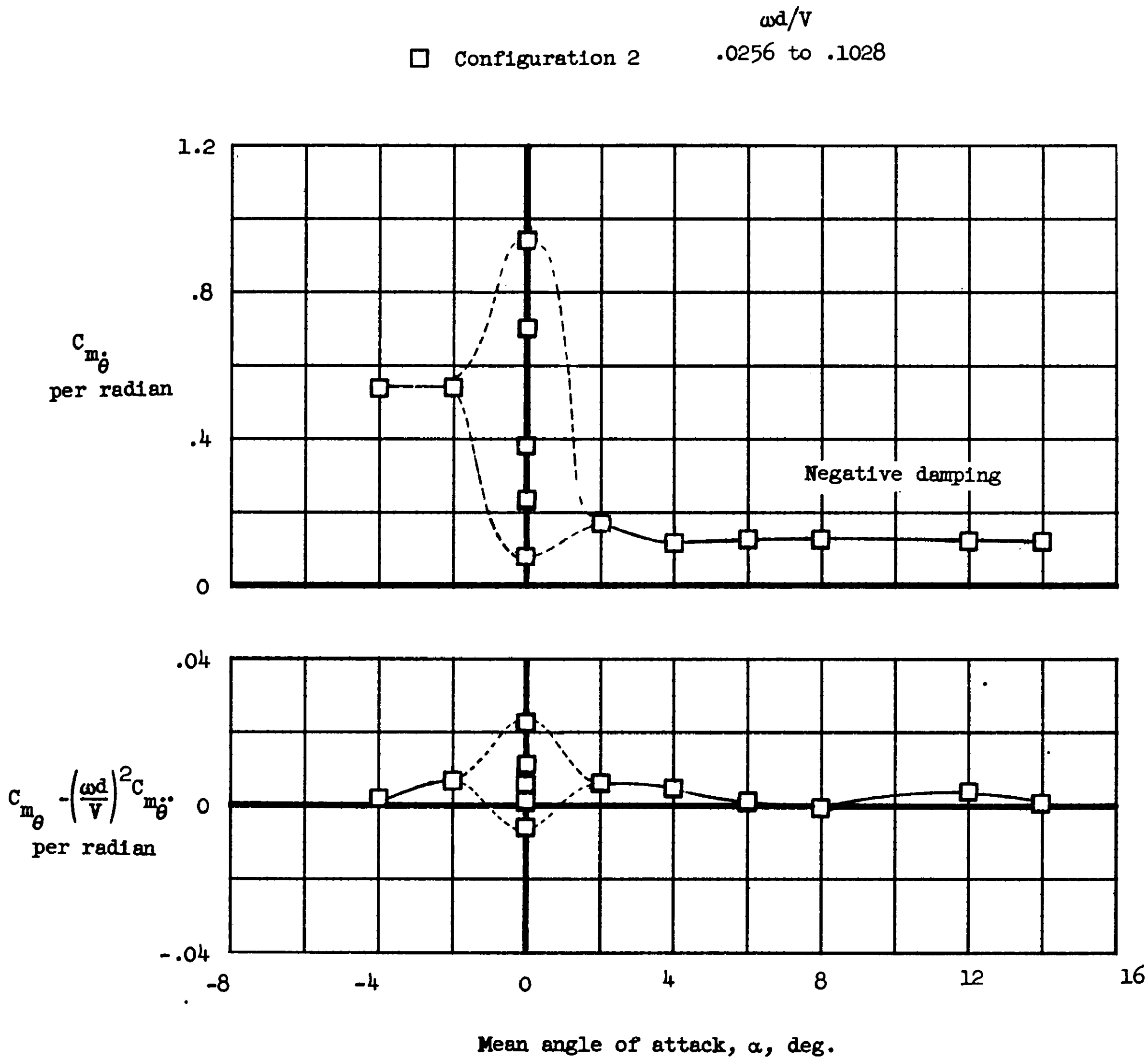

(c) M = 0.75.

Figure 5.- Continued.

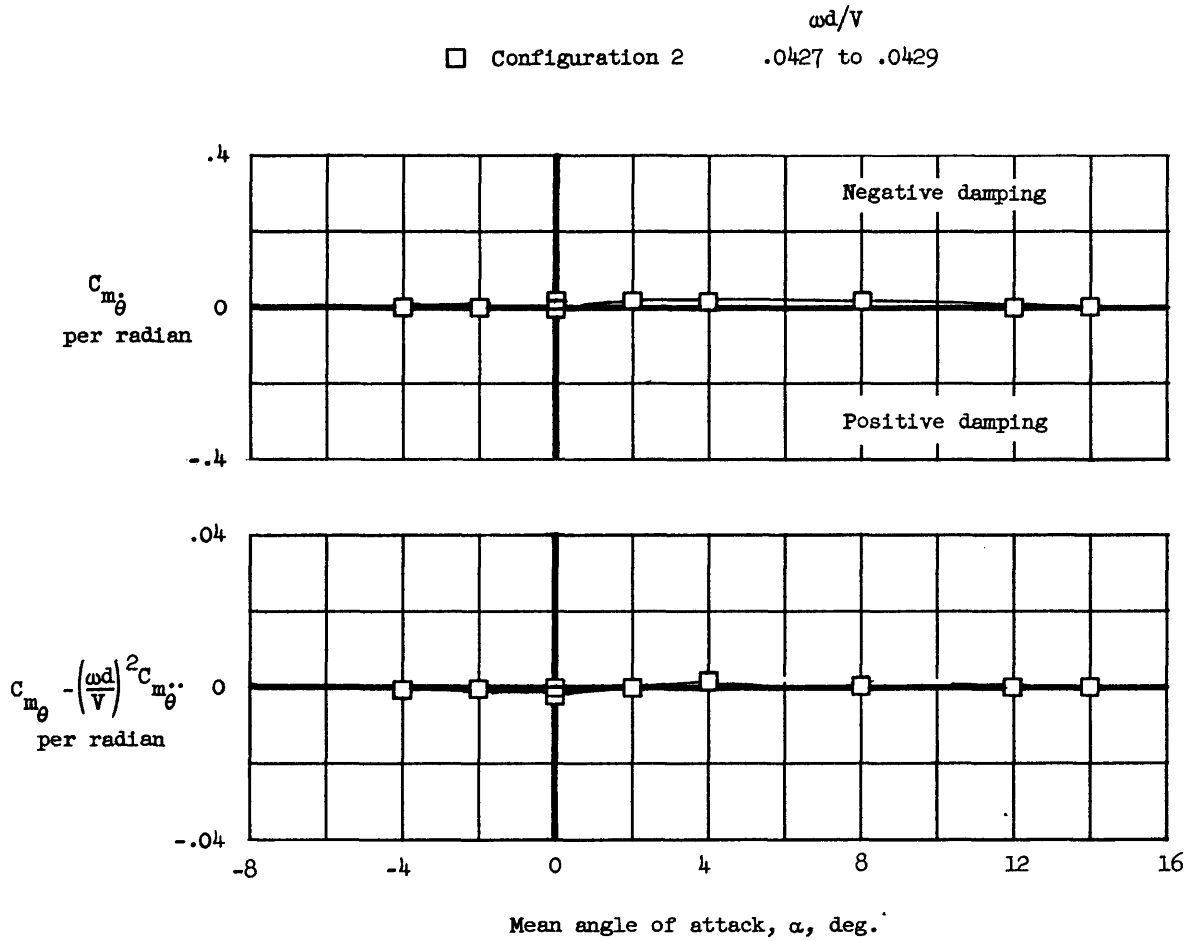

(d) M = 0.90.

Figure 5.- Continued.

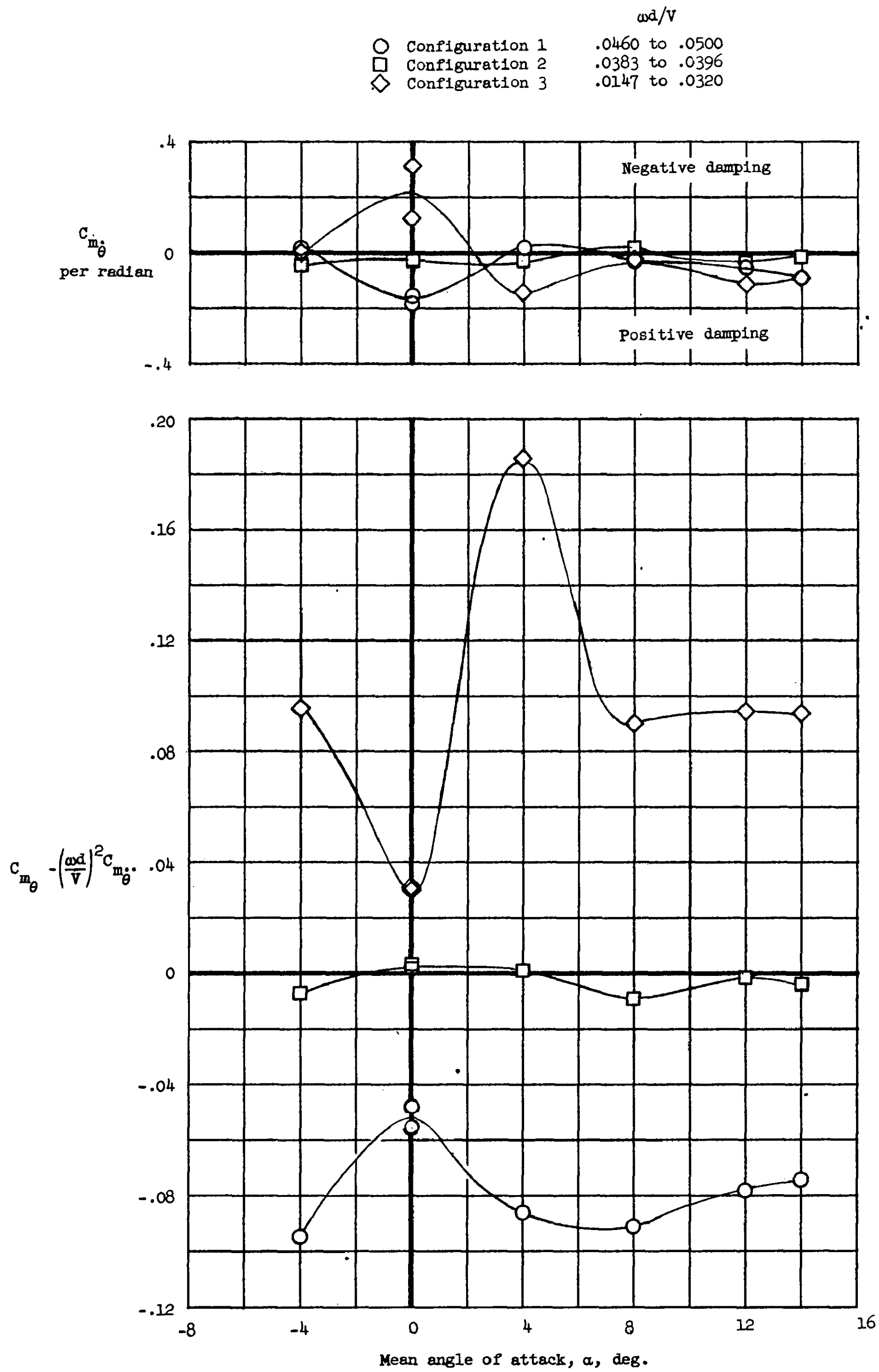

(e) M = 1.00.

Figure 5.- Continued.

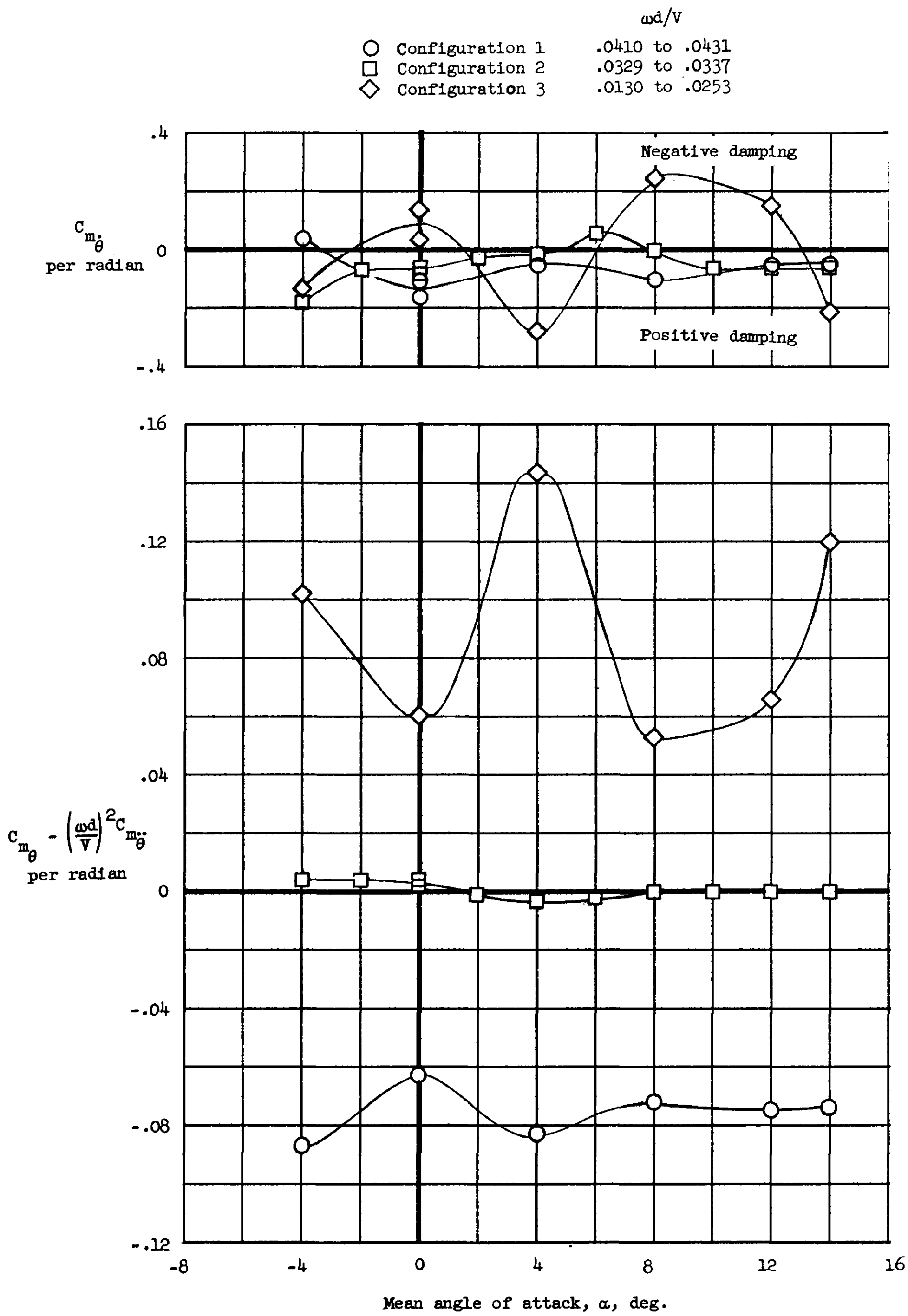

(f) M = 1.20.

Figure 5.- Continued.

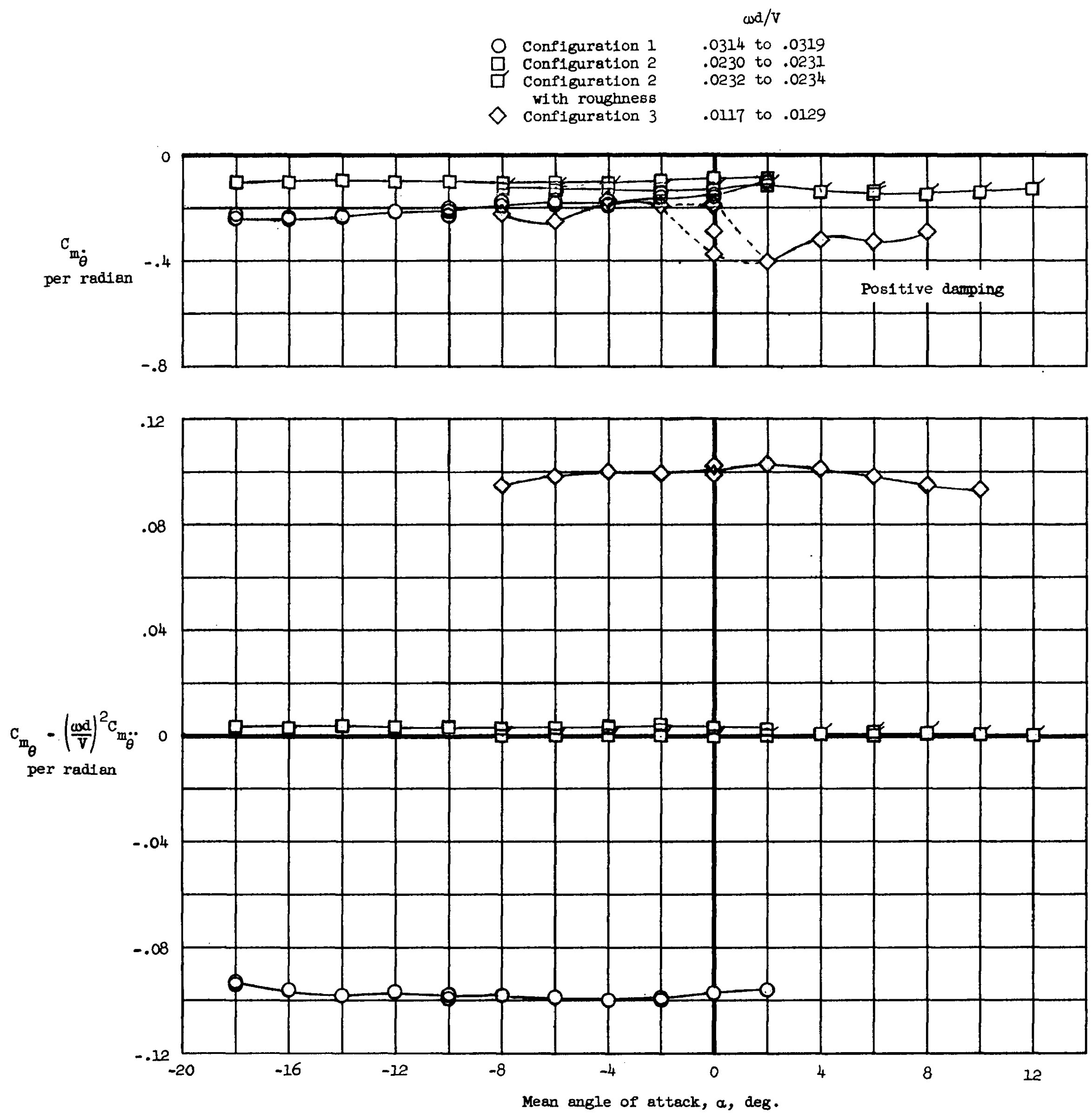

(g) M = 2.00.

Figure 5.- Continued.

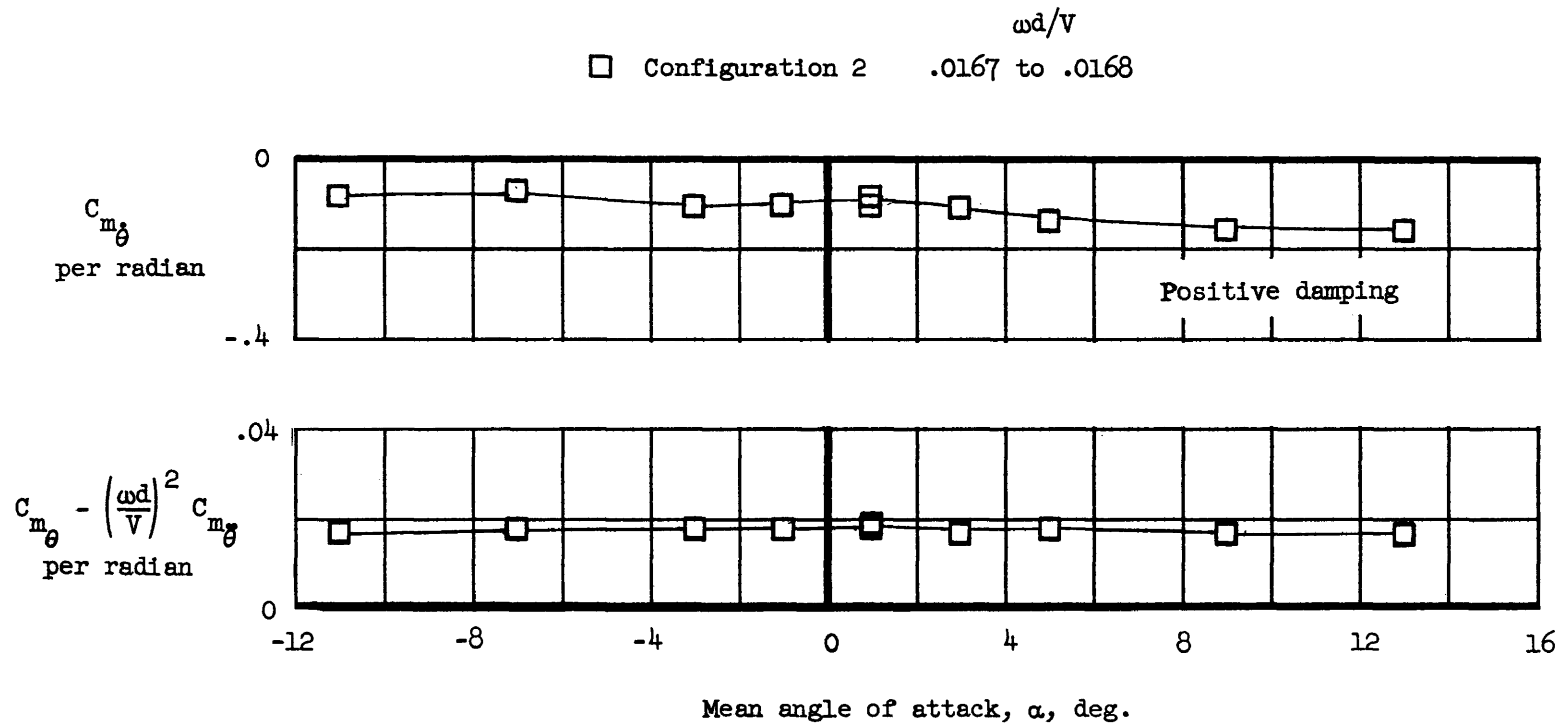

(h) M = 4.63.

Figure 5.- Concluded.

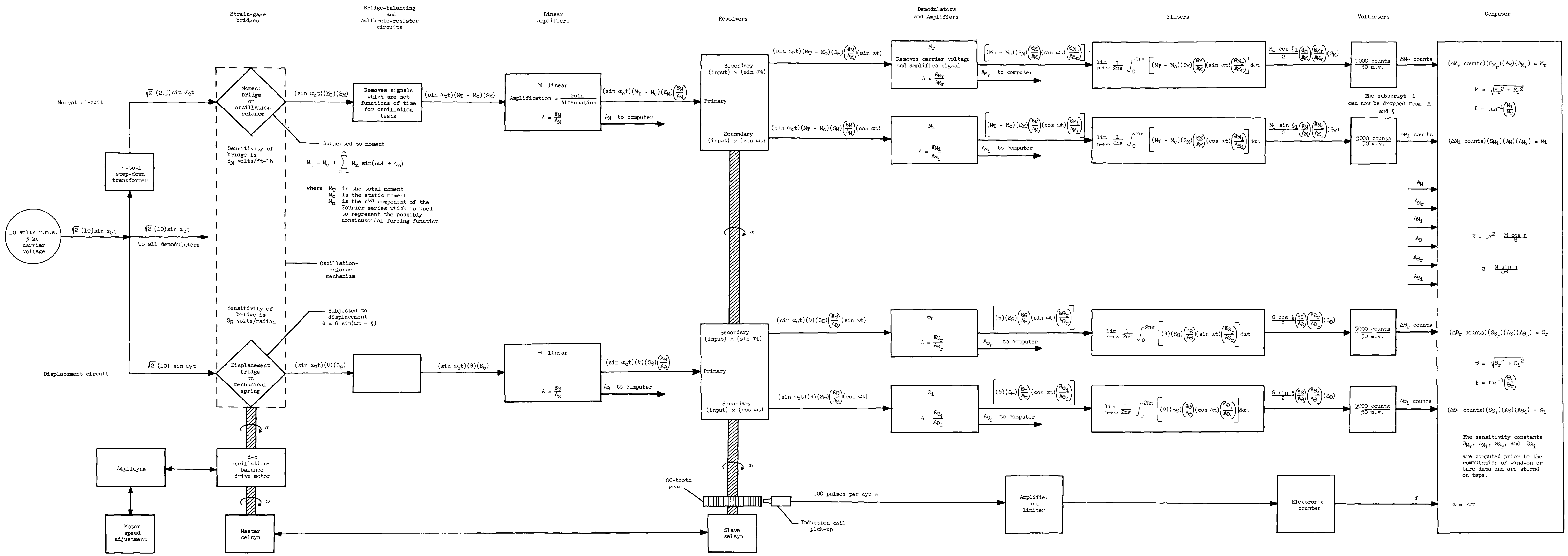

(a) Circuit used to determine M, Θ, η, and ω.

Figure 2.- Block diagram of electronic circuit.